IEEE Access
Multidisciplinary | Rapid Review | Open Access Journal

Received 2 May 2022, accepted 21 June 2022, date of publication 20 July 2022, date of current version 28 July 2022.

Digital Object Identifier 10.1109/ACCESS.2022.3192555

RESEARCH ARTICLE

Detection of Kidney Cancer Using Circularly Polarized Patch Antenna Array

DEMYANA A. SALEEB[1], REHAB M. HELMY[2], NIHAL F. F. AREED[3], MOHAMED MAREY[4], (Senior Member, IEEE), KHALED MOHAMAD ALMUSTAFA[5], AND AHMED S. ELKORANY[2]

[1]Faculty of Engineering, Kafrelsheikh University, Kafrelsheikh 33516, Egypt
[2]Faculty of Electronic Engineering, Menoufia University, Menouf 32952, Egypt
[3]Faculty of Engineering, Mansoura University, Mansoura 35516, Egypt
[4]Smart Systems Engineering Laboratory, College of Engineering, Prince Sultan University, Riyadh 11586, Saudi Arabia
[5]Department of Information Systems, College of Computer and Information Sciences, Prince Sultan University, Riyadh 11586, Saudi Arabia

Corresponding author: Demyana A. Saleeb (demyanasaleeb@eng.kfs.edu.eg)

This work was supported by the Prince Sultan University through the Article Processing Charges (APC).

ABSTRACT The use of a circularly polarized patch antenna array to detect kidney cancer by microwave techniques is proposed in this paper. A four-element linear antenna array is designed and fabricated at the ISM frequency of 2.4 GHz. The dimensions of the antenna array are 200 mm × 78 mm. The single element is a square patch with side length of 30 mm. The distance between patches is chosen to be 20 mm which ensures that mutual coupling between any two adjacent patches is less than 20 dBs. The substrate is a FR-4 material of relative permittivity 4.3 and thickness 1.6 mm. The circular polarization has an axial ratio of 0.8 dB at 2.4 GHz. The bandwidth at $S_{11} = -10$ dB is 7.23 %. Renal system phantom consisting of kidney cortex, renal capsule, ureter, adrenal gland, muscle, fat, and skin is used. Four stages of renal cancer tumors are considered depending upon the tumor size in each stage. The presence of a tumor causes an increase in the reflection coefficient (S_{11}) and a shift in resonance frequency, which can be used to identify cancer. The increase in reflection coefficient and the shift in resonance frequency are calculated for each stage of the cancer tumors. The shift in resonance frequency for the early stages is too small. Therefore, detection depends mainly on the increase in S_{11}. The shift in resonance frequency and increase in S_{11} are large for advanced stages of the tumor, which makes detection easier. Computed specific absorption rate (SAR) is found to be less than the safety levels, which means this technique is safe to use. Overall, this work suggests a new simple detection technique of kidney cancer. The advantages of this technique are: safe, compact, fast, inexpensive, comfortable examination, non-invasive, and finally non- ionizing radiation during measurement.

INDEX TERMS Circular polarization, linear antenna array, kidney cancer, renal system, S_{11}, tumor.

I. INTRODUCTION

Cancer is considered one of the fatal diseases. Cells are the fundamental units that make up the body, they grow and divide to create new cells because the body needs them. Usually, cells die once they get too old or damaged and the new cells take their place. Cancer begins when genetic changes interfere with this orderly process. Cells start to grow uncontrollably and form a mass called a tumor. A tumor is cancerous or benign: a cancerous tumor is malignant, meaning it can grow and spread to other parts of the body. A benign tumor means the tumor can grow but won't spread [1], [2]. Cancer that starts in kidney cells is named kidney or renal cancer. The main type of kidney cancer is termed renal cell carcinoma (RCC). Kidney cancer begins when healthy cells in one or both kidneys change and grow out of control, forming a mass called a renal cortical tumor.

Benign kidney tumors affect kidney function and may cause pain and other symptoms, but the cells don't spread to other organs [3]. The different methods of kidney

The associate editor coordinating the review of this manuscript and approving it for publication was Gustavo Callico.

cancer detection are either physical examinations or imaging tests [4]–[9]. Physical examinations are blood and urine tests or biopsies. These tests cannot show obviously if an individual has kidney cancer, but they sometimes give the primary hint that there is a kidney problem.

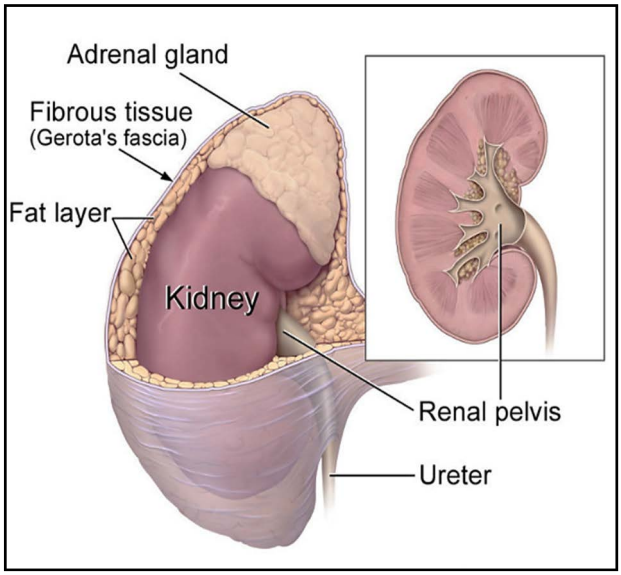

FIGURE 1. The anatomy of the left kidney including its layers [9].

Moreover, these tests are invasive and may be painful to the patient. Imaging tests include computed tomography (CT or CAT) scans, X-rays, magnetic resonance imaging (MRI), and cystoscopy [10]–[18]. The imaging techniques are highly accurate, non- invasive, determine the shape and the size of the tumor. Expensive and non- comfortable are some of its disadvantages. Recently, microwave tomography and radar-based imaging have been other ways to detect tumors [19]–[23]. These are fast, portable, and low-cost methods. The difference of dielectric properties between healthy and non-healthy tissues is the base for diagnosis in microwave systems [24], [25]. Treatment options depend on the type of cancer, its stage of diagnosis, and the patient's overall health, [26].

There are a number of papers in the literature that contain trials to detect kidney tumors and stones.

In [19] a spiral microstrip antenna was designed at (200-600) MHz. The return loss was measured in 6 malignant tissue sizes, but the difference (ΔS_{11}) was too small to detect the tumor. The shift in resonance frequency (ΔF) was measured to be 0.7, 1.4, 3.7, 4, 5.2, and 6.3 MHz due to the six malignant volume sizes. In [20] a microwave imaging using compact microstrip patch antennas is designed at different frequencies to detect kidney stones. The homogenous serum has similar dielectric properties as the normal human body was used. A calcium stone was immersed in the serum. Five various patch antennas are designed and their resonance frequencies found to be at 2.26, 2.38, 2.49, 2.5, 2.62 GHz respectively. The difference in reflection coefficient (S_{11}) was measured at these resonance frequencies to be 0.32, 2.2, 1.5, 2.5, and 5 dB respectively. A microwave imaging UWB monopole antenna was used in [21] to detect kidney stones. Water and water with calcium were used to simulate the kidney dielectric properties. A difference in S_{11} at 3.8 GHz was found to be 12 dB between water and water with calcium.

This paper is organized as follows. Section 2 gives some information about kidney anatomy, kidney cancer, and electrical properties of cancerous and normal kidney tissues. The design and fabrication of the proposed antenna is outlined in section 3. Simulation results and conclusions are given in sections 4 and 5 respectively.

II. KIDNEY ANATOMY AND KIDNEY CANCER

The kidneys are two bean-shaped organs. They sit within the body towards the center to the lower part of the back [27]. There are six layers until reaching the kidney which are skin, fat, muscle, ribs, fascia, renal capsule, and the kidney. Each kidney has on its top a gland called the adrenal gland that's in the shape of a pyramid. The dimensions of the kidney depend on the body size. A normal adult male kidney has a minimum length of 11 centimeters. A normal adult female kidney has a minimum length of 10 centimeters. The anatomy of a part of the renal system is presented in Fig.1 [28].

There are four stages for cancer tumors, [29], [30]. Knowing the stage can help choose the appropriate treatment option and may even aid in predicting the patient's state. The stage of the cancer is assigned according to its size and location. Table 1 reports the four stages. Figure 2 shows the stages of kidney cancer [31], [18].

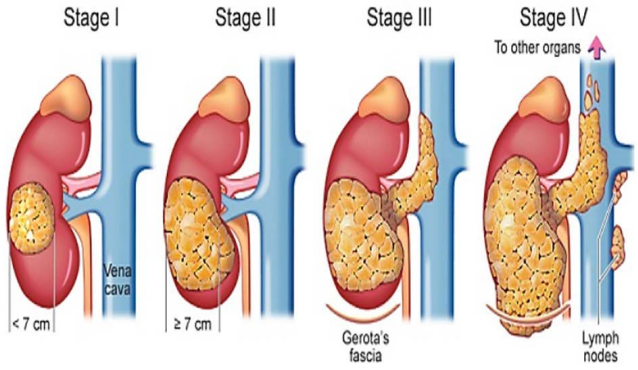

FIGURE 2. Kidney cancer stages [32].

The kidney tissues are affected by the disease and temperature. There are variations within the dielectric properties concerning the healthy tissue. In normal tissues, when the frequency increases, the conductivity increases and the permittivity falls. Malignant tissues have higher electrical properties because of higher water and sodium content [33]. Microwave techniques consider the biological tissues as dielectrics.

The electromagnetic properties of healthy human tissues within the frequency range 10 Hz to 100 GHz were given in [24], [34], [35].

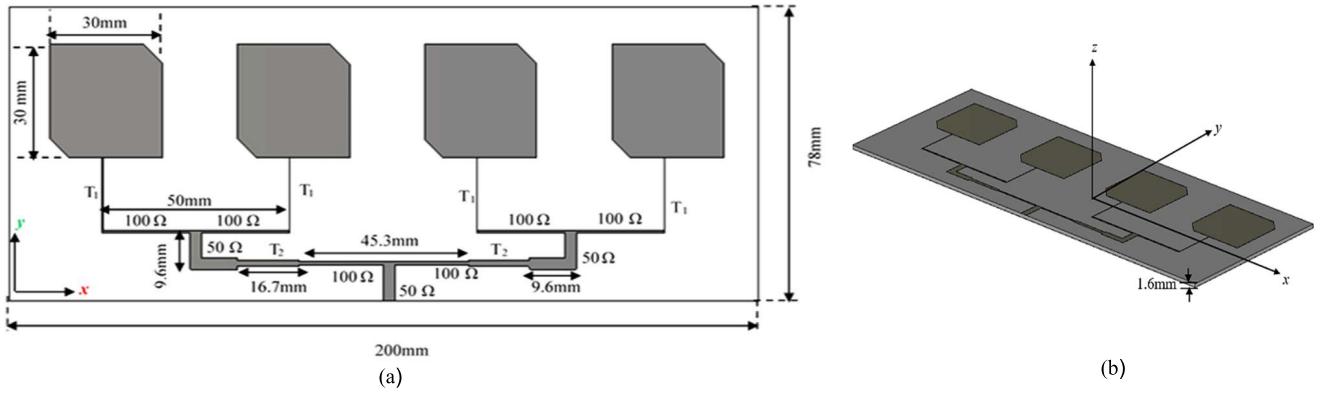

FIGURE 3. (a) Top view of the proposed CP antenna array and feeding network, (b) 3-D side view of the proposed antenna.

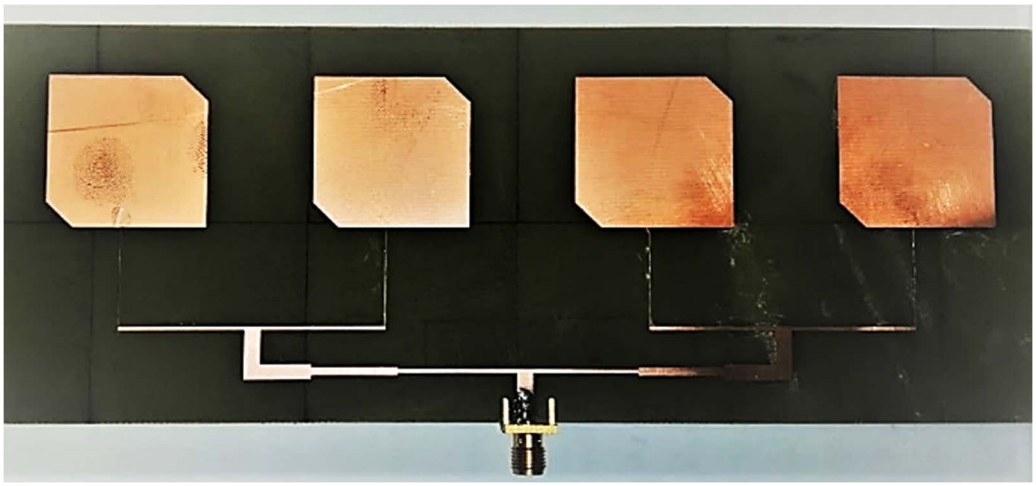

FIGURE 4. The manufactured antenna.

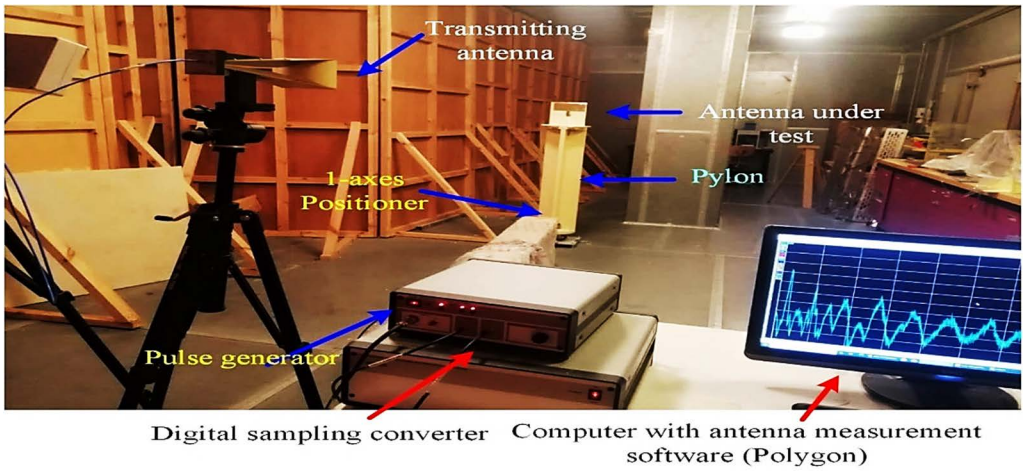

FIGURE 5. The antenna measurement setup.

Generally, in most of the examined tissues, the electrical permittivity and conductivity of the malignant tissues were higher than the traditional tissues of the same type. Kidney cancerous dielectric properties are increased by (4-6)% higher than normal cells [25]. This is because the kidney has a lot of water content in its tissue. In [37] the renal

TABLE 1. The four stages of renal cell carcinoma (RCC).

Stages	Description
Stage I	The tumor is less than 7 cm and confined to the kidney.
Stage II	The tumor is larger than 7 cm and confined to the kidney.
Stage III	The tumor reaches to one or more local lymph nodes, or the tumor is in the vein leaving the kidney going to the heart, or the tumor has spread to the fat around the kidney or the adrenal gland.
Stage IV	The kidney cancer has spread to the fat surrounding it or has spread to other body organs or distant lymph nodes.

TABLE 2. Widths of transmission lines vs. their characteristic impedances.

Characteristic impedance	Width
50 Ω	3.11mm
70.7 Ω	1.12mm
100 Ω	0.7 mm
158 Ω	0.145 mm

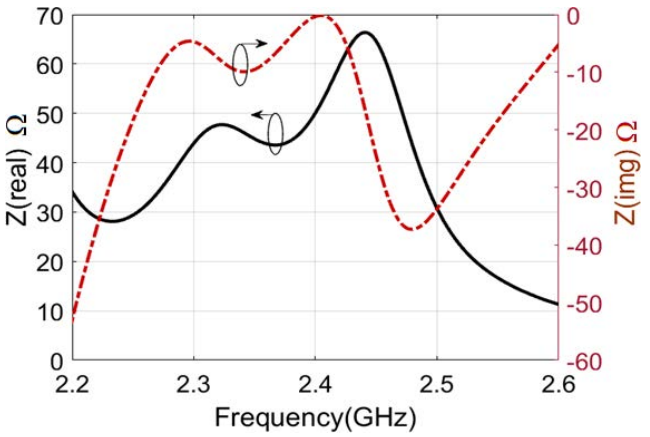

FIGURE 6. Real and imaginary parts of the input impedance of the feeding network.

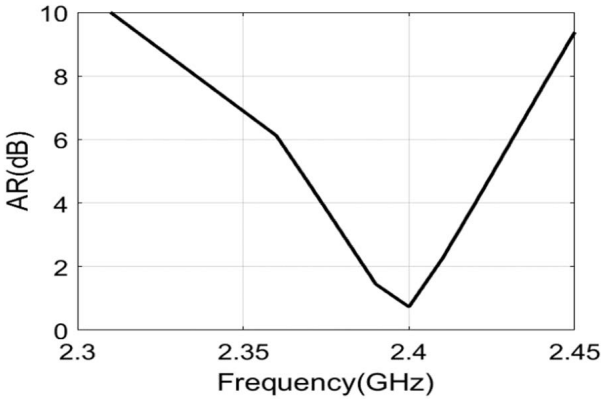

FIGURE 7. Axial ratio of the array.

dielectric properties are given in microwave range between 0.5 GHz to 8.5 GHz.

III. PROPOSED STRUCTURE

A. ANTENNA DESIGN

The antenna was designed and fabricated by the authors [38]. The geometric structure of the CP patch antenna array is shown in Fig. 3. The substrate is FR-4 its height is 1.6 mm and $(\varepsilon_r) = 4.3$ is on the top of full ground plane its thickness is 0.035mm. The overall dimension of the antenna array is 200×78 mm^2, while the square patch has a side length 30 mm. Two isosceles triangles with 5mm length of its legs are cut from the edges of the squared patch to achieve the circular polarization [39], [40]. The antenna is designed to operate in ISM band at resonance frequency 2.4 GHz.

The manufactured antenna is shown in Fig. 4. Figure 5 shows the antenna measuring system of Geozondas which is a pulse time domain measurement method [41].

To reduce mutual coupling, the distance between antenna elements were increased to 20 mm. The mutual coupling between adjacent patches was computed and found to be less than -20 dB in the desired bandwidth. The corporate feed network was designed to give good matching of the array [42]–[45].

B. THE CORPORATE FEEDING NETWORK

Figure 3 shows the corporate feeding network. The patch input impedance is given by, [38]:

$$Z_{in} = \frac{60\lambda_o}{w_1}. \quad (1)$$

where, λ_o is the wave length $= 125$ mm corresponding to the resonance frequency 2.4 GHz, while w_1 is the side length of

TABLE 3. Electrical, thermal parameters and thickness of each layer in renal system [34], [36].

Tissue	Thickness (mm)	(ε_r)	(σ)S/m	(ρ) Kg/m^3	(K) W/m/k	(C) J/Kg/k
Renal capsule (connective tissue)	0.3	43.2	1.64	1027	0.35	2372
Fatty layer (fascia)	2	10.8	2.61	911	0.21	2348
Kidney	21	52.9	2.39	1066	0.53	3763
Adrenal gland	-	58	1.06	1028	0.44	3513
Ureter	-	18	0.673	1102	0.46	3306
Muscle	14	52.8	1.71	1090	0.49	3421
Fat	11	10.8	2.61	911	0.21	2348
Skin	2	38.1	1.44	1109	0.37	3391
tumor	-	50	2.39	997	0.64	3978

TABLE 4. (ΔS_{11}) of CP and LP.

	Stage 1	Stage 2	Stage 3	Stage 4
CP (dB)	5	6.9	14.1	16.6
LP (dB)	1.1	2.8	3.9	5.8

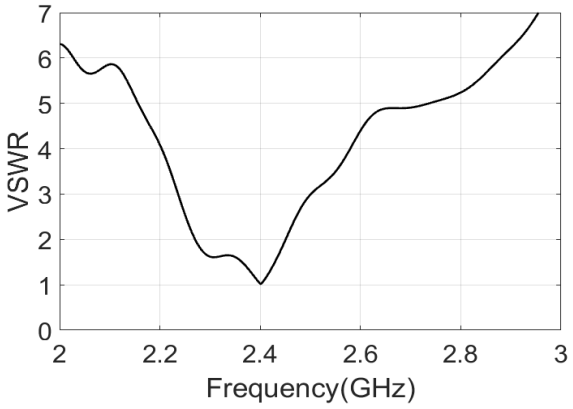

FIGURE 8. The simulated VSWR.

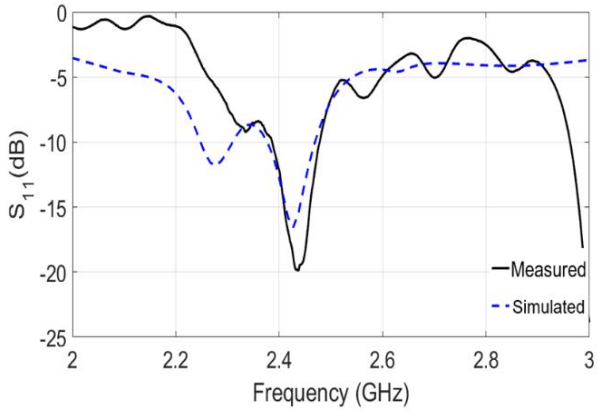

FIGURE 9. The reflection coefficient (S11): Measured and simulated.

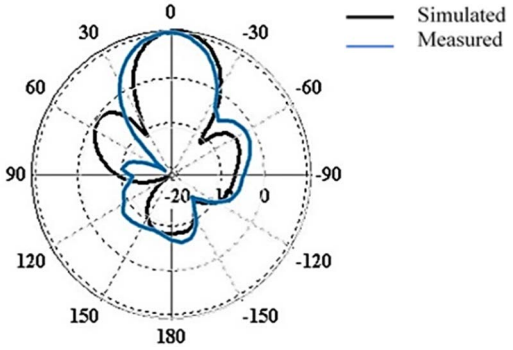

FIGURE 10. The Radiation pattern H- plane: Measured and simulated.

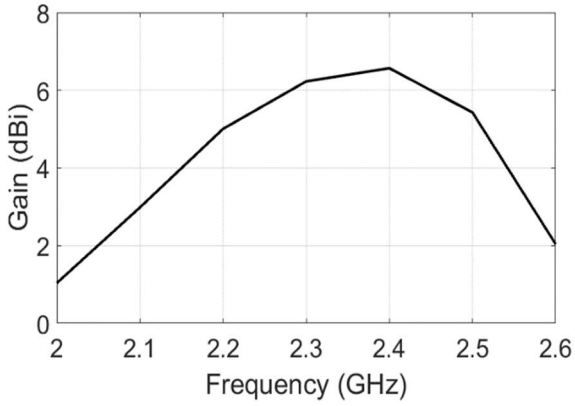

FIGURE 11. Simulated antenna gain over frequency.

the square patch = 30mm. Hence, the patch impedance = 250 Ω. However, T_1 is the quarter wave transformer that adjusts the 100 Ω transmission line to the patch. The value of its characteristic impedance can be calculated as;

$$Z_{T_1} = \sqrt{Z_{out} * Z_{in}} = \sqrt{250 * 100} = 158\Omega. \quad (2)$$

T_2 is the quarter wave transformer that joins the 50 Ω and 100 Ω transmission lines and has characteristic impedance $Z_{T2} = 70.7$ Ω.

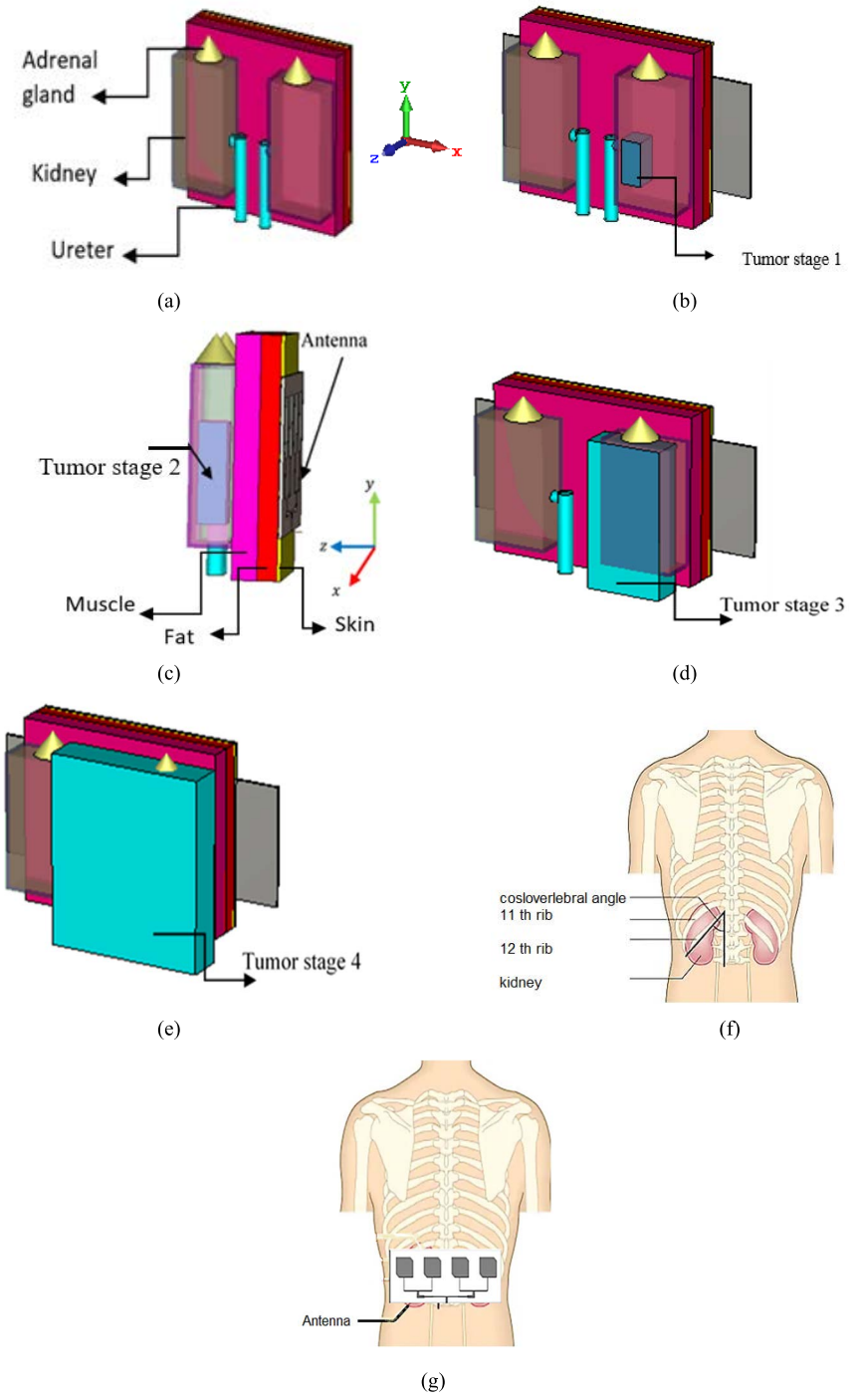

FIGURE 12. **(a) The renal phantom, (b) side view of the renal phantom with tumor stage 1 and the antenna on the phantom back skin (c) the renal phantom with tumor stage 2, (d) the renal phantom with tumor stage 3, (e) the renal phantom with tumor stage 4, (f) kidneys position at human body, (g) position of the antenna on human back.**

W_2 is the width of the transmission line with characteristic impedance Z_o, calculated as, [39]:

$$\frac{W_2}{h} = \frac{2}{\pi}\left\{\{\frac{\varepsilon_r - 1}{2\varepsilon_r}\left[\ln(B-1) - \frac{0.61}{\varepsilon_r} + 0.39\right] + B - 1 - \ln(2B-1)\right\}. \quad \text{for } A < 1.52 \tag{3}$$

or,

$$\frac{W_2}{h} = \frac{8e^A}{e^{2A} - 2}, \quad \text{for } A < 1.52 \tag{4}$$

where,

$$A = \frac{Z_o}{60}\sqrt{\{\frac{\varepsilon_r + 1}{2}\}^{1/2}} + \frac{\varepsilon_r - 1}{\varepsilon_r + 1}\left\{\frac{0.11}{\varepsilon_r} + 0.23\right\}, \tag{5}$$

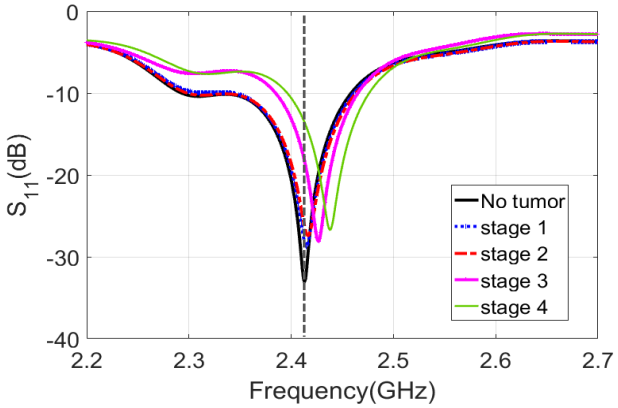

FIGURE 13. The reflection coefficient of the four stages of tumor size and no tumor in CP antenna array.

and,

$$B = \frac{529.18}{Z_o\sqrt{\varepsilon_r}}. \tag{6}$$

The optimized widths of the transmission lines 50Ω,70.7Ω, 100 Ω and 158 Ω are shown in Table 2.

The input impedance of the antenna array is simulated by CST microwave studio. Figure 6 shows the real and imaginary parts which are 50 and 0 Ω respectively at 2.4 GHz. Perfect matching is achieved.

There is the near field phase corrected antenna which gives circular polarization and avoids the feeding network [46], [47]

C. ANTENNA CHARACTERISTICS

The antenna is simulated using CST. The axial ratio is shown in Fig. 7. Excellent impedance matching of the proposed antenna at 2.4 GHz with 7.3 % impedance bandwidth (from 2.274 GHz to 2.4474 GHz) can be noticed. The polarization bandwidth is 1.7% (axial ratio under 3 dB).

Circular polarization increases ΔS_{11} which increases the probability of tumor detection. Table (4) compares ΔS_{11} for circular and linear polarizations. Thus, circular polarization is much better than linear polarization in tumor detection. Figure 8 shows the simulated VSWR which equals 1 at 2.4 GHz. Figure 9 depicts measured and simulated S_{11}. Both simulated and measured S_{11} are identical at 2.4 GHz. Figure 10 depicts the radiation pattern (E- plane). Between the measured and simulated major lobes, there is relatively little difference. Fabrication tolerances are to blame for this. Gain at the range of frequencies is shown in Fig. 11 with 6.6 dBi at 2.4 GHz.

IV. SIMULATION RESULTS

The antenna array is put on the body phantom including kidney. The reflection coefficient (S_{11}) is simulated by CST microwave studio for kidney tumor and without tumor.

Figure 12 (a) illustrates the configuration of the two kidneys and the renal system phantom. The side view of the

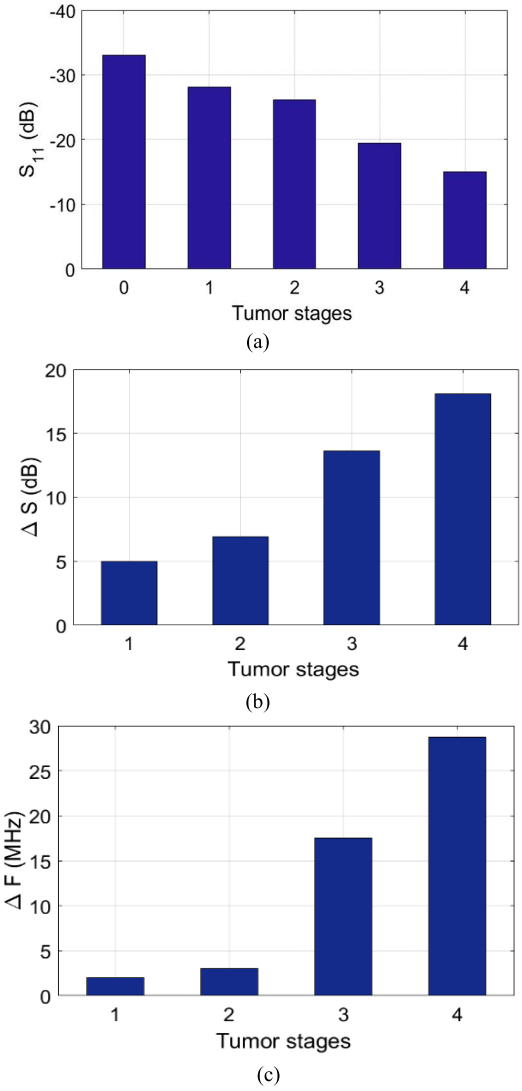

FIGURE 14. (a) S_{11} of CP antenna, (b) ΔS_{11}, and (c) The shift in resonance frequency at 2.4 GHz.

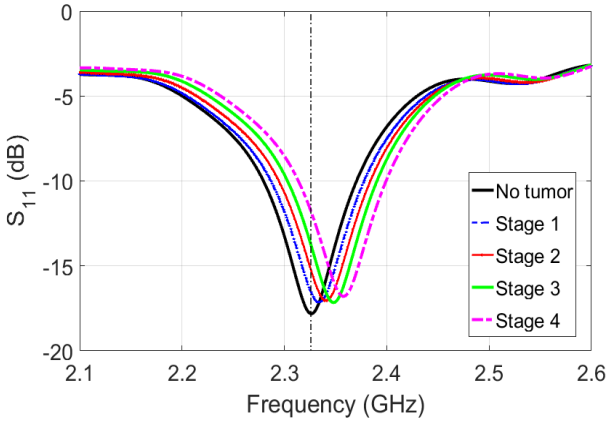

FIGURE 15. The reflection coefficient of the four stages of tumor size and.

renal phantom with tumor at the first, second, third, and fourth stages and the antenna array on the back skin are shown in Figs. 12(b),12(c), 12(d), and 12(e) respectively.

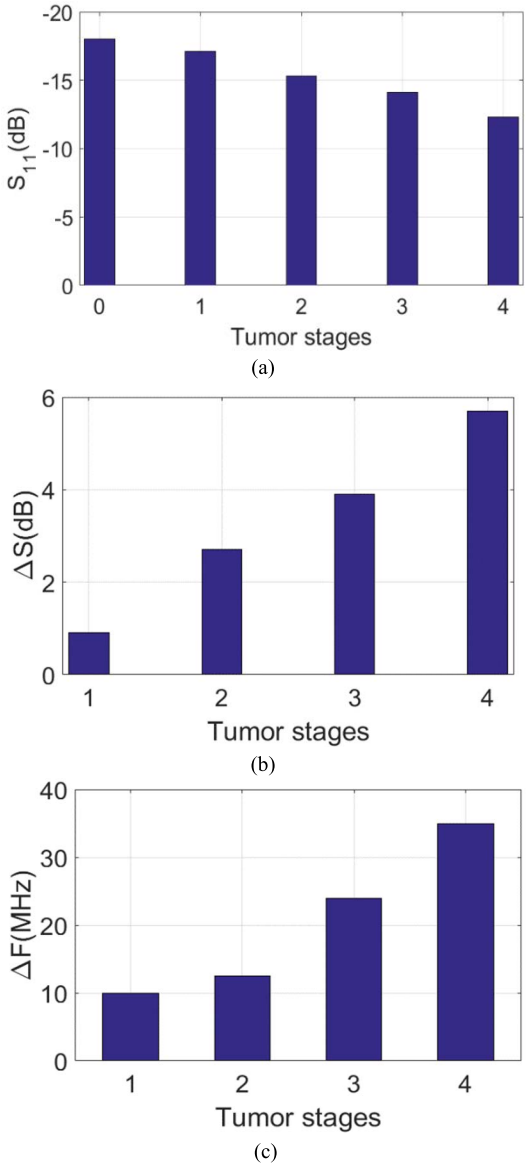

FIGURE 16. S_{11} of CP antenna, (b) ΔS_{11} (c) The shift in resonance frequency at 2.3 GHz.

Figure 12 (f) shows the position of the two kidneys in the human body. Figure 12 (g) shows the antenna array on the skin of the human back. The renal phantom consists of several layers, the thickness of each layer, the electrical, and thermal properties of each layer at 2.4 GHz are presented in Table 3. The dielectric properties of the kidney tumor at 2.4 GHz are $\varepsilon_r = 50$ and $\sigma = 2.39$ S/m [25], [36], [37].

S_{11} was simulated for each stage of the kidney tumor and compared with the case of no tumor.

Figure 13 displays the results of S_{11} for no tumor and the four stages of tumor size. The presence of a tumor has two effects: first, it raises the S_{11} level, and second, it shifts the resonance frequency.

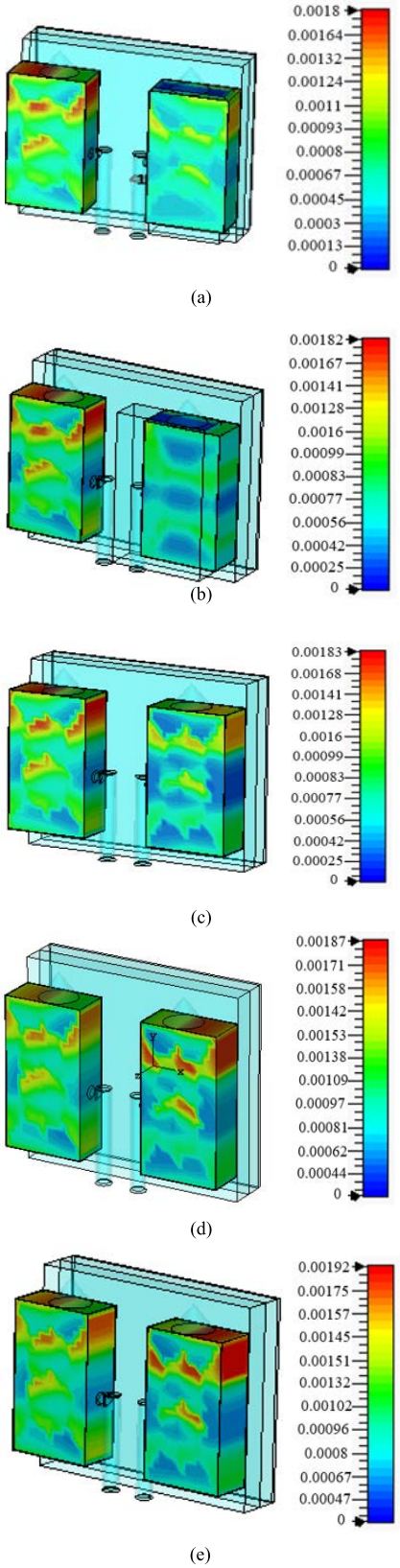

FIGURE 17. SAR values for kidney phantom (a) without tumor, (b) stage 1, (c) stage 2, (d) stage 3, (e) stage 4.

TABLE 5. A comparison of kidney cancer published works and the proposed work.

Published researches	Technique	Utilization in diagnosis	Advantages	Antenna dimensions	Frequency band	Results
[19]	Microwave techniques • ΔS_{11} • ΔF	• Based on the difference between the dielectric properties of healthy and malignant tissues. • Measure the difference in S_{11} and shift in resonance frequency with and without tumor.	• Portable. • Safe • Compact. • Fast. • Low cost. • Non-invasive. • Comfortable examinations.	A logarithmic spiral microstrip antenna its dimension is 11× 6 × 1.9 mm^3	(200-600) MHz At fr =403MHz	The difference in S11 is too small to detect kidney tumors.
[20]	Microwave techniques • ΔS_{11}	• Measure the difference in S_{11} between the homogenous serum and the calcium stone.	• Portable. • Safe • Compact. • Fast. • Low cost. • Non-invasive.	6 various compact microstrip patch antennas	ISM band at 2.4 GHz	kidney stone detection can be diagnosis by the difference in S11,
[21]	Microwave techniques • ΔS_{11}	• Measure the difference in S_{11} between water and water with calcium.	• Portable. • Safe • Compact. • Fast. • Low cost. • Non-invasive.	A monopole antenna its dimension 17.5× 17.5× 0.8 mm^3	UWB (3-11) GHz	kidney stone is detected by the difference in S11, ΔS_{11} is 12 dB in case of stone
[22]	Microwave techniques • ΔS_{11} • ΔF	• Measure the difference in S_{11} and shift in resonance frequency with 6-voulmes of tumor and without tumor.	• Small size. • Safe • Fast. • Low cost. • Non-invasive. • Comfortable examinations.	An implemented monopole antenna with dimension 14 ×10 ×0.805 mm^3	(300-500) MHz, fr= 403.2 MHz.	As the volume of malignant tissue increase from 0 mm^3 to 8076 mm^3 the frequency shift from 403.2 MHz to 392 MHz.
Proposed technique	Microwave techniques • ΔS_{11} • ΔF	• Based on the difference between the dielectric properties of kidney tumor and healthy tissues. • Measure the difference in S_{11} and shift in resonance frequency with and without tumor.	• Portable. • Safe • Fast. • Low cost. • Non-invasive. • Comfortable examinations. • Non- ionizing radiation during measurement. • Sensitive to predict small tumor.	A CP antenna array its dimension is 200 ×78× 1.5 mm^3	(2-3) GHz, fr=2.4 GHz at ISM band.	Kidney tumor is detected by 4 ×1 CP linear antenna array with Δ S11 are 5, 6.9, 14.1, and 16.6 dB respectively for the 4 stages of tumor size. ΔF was 2, 3, 18, and 28 MHz respectively in the 4 stages of tumor size.

Figure 14 shows S_{11} (a), ΔS_{11}(b), and the shift in resonance frequency (c) for the four stages of the tumor and the case of no tumor at 2.4 GHz. An increase in S_{11} and shift in resonance frequency enable detection of cancer even in its early stages. The shift in resonance frequency for stages 1 and 2 is too small. Therefore, cancer detection depends upon the increase in S_{11} which is 5 and 6.9 dBs, respectively. The increase in S_{11} for stages 3 and 4 is 14.1 and 16.6 dBs, and the shift in resonance frequency is 18 and 28 MHz, respectively. The technique presented here detects advanced stages of cancer easily. But it can also detect the early stages of the tumor. Figure 15 presents the results of S_{11} of linearly polarized antenna array (LP). The LP antenna resonates at 2.3 GHz in free space. The antenna is put on the kidney phantom. The reflection coefficient is simulated in CST at without tumors and with tumors in the four stages. Figure 16(a) summarizes the value of S_{11} in the four stages and without tumor. In Fig.16 (b) the difference in $S_{11}(\Delta S)$ between no tumor and every stage is showed. Fig 16 (c) sets the value of the shift in frequency (ΔF) between each stage of tumor and the kidney phantom without tumors.

The values of the specific absorption rate (SAR) are calculated when the power at the input terminals of the antenna was 0.5 watt. SAR is a measure of the rate of energy absorbed

per unit mass by a human body when exposed to a radio frequency (RF) electromagnetic field. It is defined as the power absorbed per unit mass of tissue and has units of watts per kilogram (W/kg). The values of SAR can be categorized as 1g or 10g mass of tissue which equivalence to 1g or 10g spatial average SAR. According to IEEE C95.1:1999; 1.6 W/Kg is the limit value for 1g spatial average SAR while it has been updated as 2 W/Kg for 10g spatial average SAR based on IEEE C95.1:2005, [48]. SAR is calculated by the formula:

$$SAR = \frac{\sigma |E|^2}{\rho}. \tag{7}$$

where, E is the maximum electric field in (V/m), σ is the electric conductivity of the tissue in (S/m), and ρ is the mass density of the tissue in Kg/m^3.

Figure 17 presents the results of the specific absorption rate (SAR) for 10g of tissue for each of the stages of tumor size in the kidney phantom and without tumor. The SAR values are computed 1.8, 1.82, 1.83, 1.87, and 1.92 mW/Kg for without tumors, tumors in stages 1, 2, 3, and 4, respectively. It is obvious that the SAR increases as the tumor size grows. The values of SAR are less than the safety rates. This means that the technique is safe to use with humans.

Table 5 above presents a comparison between different techniques used for kidney cancer detection, and the proposed technique the comparison includes how the technique is used for diagnosis frequency band, antenna used and advantages of each technique

V. CONCLUSION

This research highlighted a method for detecting kidney tumors. The design and fabrication of a circularly polarized 4 × 1 patch antenna array is reported. The detection method is based on the differences in electrical characteristics between normal and malignant kidney tissues. Kidney cancer is divided into four phases. For each stage of tumor size, the reflection coefficient is determined and compared to a case with no tumor. At 2.4 GHz, the S_{11} for the four stages of cancer are 5, 6.9, 14.1, and 16.6 dB, respectively. For the four stages, there is also a shift in resonance frequency of 2, 3, 18, and 28 MHz, respectively. In its advanced stages 3 and 4, the tumor is simple to detect. LP antenna was simulated and calculated ΔS_{11}, and the shift in frequency at 2.3 GHz. The increase in S_{11} of CP than LP was 455.6%, 155.6 %, 261.5 %, and 186.2 % form stage 1 to stage 4 respectively. Detection of early stages of the tumor depends mainly upon increase in the reflection coefficient. Specific absorption rate (SAR) was calculated for each stage and without tumor. The SAR values are below the safety limits, so the technique is safe to use. Future work in this area should include the application of the technique to real humans for more accurate diagnosis.

REFERENCES

[1] L. Wang, "Microwave sensors for breast cancer detection," *Sensors*, vol. 18, no. 2, p. 655, Feb. 2018.

[2] R. L. Siegel, K. D. Miller, and A. Jemal, "Cancer statistics," *CA Cancer J. Clin.*, vol. 67, no. 3, pp. 177–193, 2017.

[3] W. M. Linehan, J. Vasselli, R. Srinivasan, M. M. Walther, M. Merino, P. Choyke, C. Vocke, L. Schmidt, J. S. Isaacs, G. Glenn, and J. Toro, "Genetic basis of cancer of the kidney: Disease-specific approaches to therapy," *Clin. Cancer Res.*, vol. 10, no. 18, p. 6282S, Sep. 2004.

[4] K. Bluemke, U. Bilkenroth, A. Meye, S. Fuessel, C. Lautenschlaeger, S. Goebel, A. Melchior, H. Heynemann, P. Fornara, and H. Taubert, "Detection of circulating tumor cells in peripheral blood of patients with renal cell carcinoma correlates with prognosis," *Cancer Epidemiol., Biomarkers Prevention*, vol. 18, no. 8, pp. 2190–2194, Aug. 2009.

[5] O. Falegan, M. Ball, R. Shaykhutdinov, P. Pieroraio, F. Farshidfar, H. Vogel, M. Allaf, and M. Hyndman, "Urine and serum metabolomics analyses may distinguish between stages of renal cell carcinoma," *Metabolites*, vol. 7, no. 1, p. 6, Feb. 2017.

[6] P. V. Nuzzo, J. E. Berchuck, K. Korthauer, S. Spisak, A. H. Nassar, S. A. Alaiwi, A. Chakravarthy, S. Y. Shen, Z. Bakouny, F. Boccardo, and J. Steinharter, "Detection of renal cell carcinoma using plasma and urine cell-free DNA methylomes," *Nature Med.*, vol. 26, no. 7, pp. 1041–1043, Jul. 2020.

[7] J. T. Leppert, J. Hanley, T. H. Wagner, B. I. Chung, S. Srinivas, G. M. Chertow, J. D. Brooks, and C. S. Saigal, "Urologic diseases in America project. utilization of renal mass biopsy in patients with renal cell carcinoma," *Urology*, vol. 1, vol. 83, no. 4, pp. 774–780, Apr. 2014.

[8] H. D. Patel, M. H. Johnson, P. M. Pierorazio, S. M. Sozio, R. Sharma, E. Iyoha, E. B. Bass, and M. E. Allaf, "Diagnostic accuracy and risks of biopsy in the diagnosis of a renal mass suspicious for localized renal cell carcinoma: Systematic review of the literature," *J. Urol.*, vol. 195, no. 5, pp. 1340–1347, May 2016.

[9] National Institute. (2007). *Kidney and Adrenal Gland*. Accessed: Nov. 28, 2020. [Online]. Available: https://visualsonline.cancer.gov/details.cfm?imageid=4355

[10] S. Mihara, K. Kuroda, R. Yoshioka, and W. Koyama, "Early detection of renal cell carcinoma by ultrasonographic screening based-on the results of 13 years screening in Japan," *Ultrasound Med. Biol.*, vol. 25, no. 7, pp. 1033–1039, Sep. 1999.

[11] S. S. Sagel, R. J. Stanley, R. G. Levitt, and G. Geisse, "Computed tomography of the kidney," *Radiology*, vol. 124, no. 2, pp. 359–370, Aug. 1977.

[12] B. H. Doornweerd, I. J. de Jong, L. M. Bergman, and H. J. Ananias, "Chest X-ray in the follow-up of renal cell carcinoma," *World J. Urol.*, vol. 32, no. 4, pp. 1015–1019, Aug. 2014.

[13] I. Pedrosa, D. C. Alsop, and N. M. Rofsky, "Magnetic resonance imaging as a biomarker in renal cell carcinoma," *Cancer*, vol. 15, no. 115, pp. 2334–2345, May 2009.

[14] A. W. Leung, G. M. Bydder, R. E. Steiner, D. J. Bryant, and I. R. Young, "Magnetic resonance imaging of the kidneys," *Amer. J. Roentgenol.*, vol. 143, no. 6, pp. 1215–1227, Dec. 1984.

[15] S. K. Kang, M. A. Bjurlin, and W. C. Huang, "Management of small kidney tumors," *J. Amer. Med. Assoc.*, vol. 321, no. 16, pp. 1622–1623, Apr. 2019.

[16] C. R. Divgi, R. G. Uzzo, C. Gatsonis, R. Bartz, S. Treutner, J. Q. Yu, D. Chen, J. A. Carrasquillo, S. Larson, P. Bevan, and P. Russo, "Positron emission tomography/computed tomography identification of clear cell renal cell carcinoma: Results from the REDECT trial," *J. Clin. Oncol.*, vol. 31, no. 2, p. 187, Jan. 2013.

[17] R. S. Matulewicz, J. O. DeLancey, and J. J. Meeks, "Cystoscopy," *J. Amer. Med. Assoc.*, vol. 317, no. 11, p. 1187, 2017.

[18] S. B. Hancock and C. S. Georgiades, "Kidney cancer," *Cancer J.*, vol. 22, no. 6, pp. 387–392, Nov. 2016.

[19] M. H. Hassan and A. M. M. A. Allam, "Effect of kidney malignant tissues on antenna resonance," *Universal J. Biomed. Eng.*, vol. 2, no. 1, pp. 1–4, Jan. 2014.

[20] M. Alwan and S. Sadek, "Investigation of kidney stone using a microstrip patch antenna scanning system," *Abstract Emerg. Trends Sci. Res.*, vol. 4, pp. 1–26, Jun. 2015.

[21] A. J. Al-Gburi, I. Ibrahim, and Z. Zakaria, "A miniature raspberry shaped UWB monopole antenna based on microwave imaging scanning technique for kidney stone early detection," *Int. J. Psychosoc. Rehabil.*, vol. 24, no. 2, pp. 1755–1763, Apr. 2020.

[22] A. Bouazizi, G. Zaibi, A. Iqbal, A. Basir, M. Samet, and A. Kachouri, "A miniaturized implantable monopole antenna design for kidney cancer detection," *World J. Model. Simul.*, vol. 16, no. 1, pp. 3–10, 2020.

[23] S. N. Muhammad, M. M. Isa, and F. Jamlos, "Review article of microwave imaging techniques and dielectric properties for lung tumor detection," *AIP Conf.*, vol. 2203, no. 1, 2020, Art. no. 020012.
[24] D. Miklavčič, N. Pavšelj, and F. X. Hart, "Electric properties of tissues," in *Wiley Encyclopedia of Biomedical Engineering*. Hoboken, NJ, USA: Wiley, 2006.
[25] W. T. Joines, Y. Zhang, C. Li, and R. L. Jirtle, "The measured electrical properties of normal and malignant human tissues from 50 to 900 MHz," *Med. Phys.*, vol. 21, no. 4, pp. 547–550, 1994.
[26] B. Escudier and A. Mejean, *A Better Understandind of Kidney Cancer*. Paris, France: John Libbey Eurotext, 2011.
[27] M. A. Wallace, "Anatomy and physiology of the kidney," *AORN J.*, vol. 68, no. 5, pp. 799–820, Nov. 1998.
[28] R. M. Soriano and S. W. Leslie, *Anatomy, Abdomen and Pelvis, Kidneys*. Tampa, FL, USA: StatPearls, 2019.
[29] S. A. Emamian, M. B. Nielsen, J. F. Pedersen, and L. Ytte, "Kidney dimensions at sonography: Correlation with age, sex, and habitus in 665 adult volunteers," *Amer. J. Roentgenol.*, vol. 160, no. 1, pp. 83–86, 1993.
[30] B. Ljungberg, D. C. Hanbury, M. A. Kuczyk, and A. S. Merseburger, *Guidelines on Renal Cell Carcinoma*. Arnhem, The Netherland: Uroweb, 2013.
[31] F. F. Marshall, A. K. Stewart, and H. R. Menck, "The national cancer data base: Report on kidney cancers. Cancer," *Interdiscipl. Int. J. Amer. Cancer Soc.*, vol. 80, no. 11, pp. 2167–2174, 1997.
[32] *Kidney Cancer Stages, Kidney Cancer Diagnosis and Treatments, Cancer Diet*. Accessed: Nov. 28, 2020. [Online]. Available: https://cancerdiet.com/kidney-cancer/
[33] F. H. Cornelis, C. Marcelin, and J. C. Bernhard, "Microwave ablation of renal tumors: A narrative review of technical considerations and clinical results," *Diagnostic Intervent. Imag.*, vol. 98, no. 4, pp. 287–297, 2017.
[34] C. Gabriel, "Compilation of the dielectric properties of body tissues at RF and microwave frequencies," Dept. Phys., King's College London, London, U.K., Tech. Rep. ADA303903, 1996.
[35] S. N. Muhammad, M. M. Isa, and F. Jamlos, "Review article of microwave imaging techniques and dielectric properties for lung tumor detection," *AIP Conf., Proc.*, vol. 2203, no. 1, 2020, Art. no. 020012.
[36] IT'IS Foundation. *Tissue Properties Database. Version 3.1*. [Online]. Available: https://itis.swiss/virtual-population/tissue-properties/downloads/database-v3-1/
[37] A. La Gioia, A. Elahi, A. Bottiglieri, N. Ištuk, C. Dowling, F. D'Arcy, M. O'Halloran, and E. Porter, "Early-stage dielectric characterization of renal cell carcinoma for positive surgical margin detection," in *Proc. 13th Eur. Conf. Antennas Propag. (EuCAP)*, 2019, pp. 1–5.
[38] D. A. Saleeb, R. M. Helmy, N. F. F. Areed, M. Marey, W. M. Abdulkawi, and A. S. Elkorany, "A technique for the early detection of brain cancer using circularly polarized reconfigurable antenna array," *IEEE Access*, vol. 9, pp. 133786–133794, 2021.
[39] G. S. Kirov, "Evaluation of the frequency bandwidth and gain properties of antennas: Characteristics of circularly polarized microstrip antennas," *IEEE Antennas Propag. Mag.*, vol. 62, no. 3, pp. 74–82, Mar. 2020.
[40] Z. Muludi and B. Aswoyo, "Truncated microstrip square patch array antenna 2×2 elements with circular polarization for S-band microwave frequency," in *Proc. Int. Electron. Symp. Eng. Technol. Appl. (IES-ETA)*, Sep. 2017, pp. 87–92.
[41] *Antenna Measurement Without an Anechoic Chamber*. Accessed: Jun. 2021. [Online]. Available: https://geozondas.com/main_page.php?pusl=12
[42] J. Zhang, J. Li, and J. Chen, "Mutual coupling reduction of a circularly polarized four-element antenna array using metamaterial absorber for unmanned vehicles," *IEEE Access*, vol. 7, pp. 57469–57475, 2019.
[43] B. Mohamadzade, A. Lalbakhsh, R. B. Simorangkir, A. Rezaee, and R. M. Hashmi, "Mutual coupling reduction in microstrip array antenna by employing cut side patches and EBG structures," *Prog. Electromagn. Res. M*, vol. 89, pp. 87–179, 2020.
[44] H. Kondori, M. A. Mansouri-Birjandi, and S. Tavakoli, "Reducing mutual coupling in microstrip array antenna using metamaterial spiral resonator," *Int. J. Comput. Sci. Issues*, vol. 9, no. 3, p. 51. May 2012.
[45] M. Alibakhshikenar, F. Babaeian, B. S. Virdee, and S. Aissa, "Various decoupling mechanisms with focus on metamaterial and metasurface principles applicable to SAR and MIMO antenna systems," *IEEE Access*, vol. 8, pp. 192965–193004, 2020.
[46] F. Ahmed, M. U. Afzal, T. Hayat, K. P. Esselle, and D. N. Thalakotuna, "A dielectric free near field phase transforming structure for wideband gain enhancement of antenna," *Sci. Rep.*, vol. 11, p. 14613. Accessed: Mar. 25, 2022. [Online]. Available: https://www.nature.com/
[47] M. U. Afzal and K. P. Esselle, "A low-profile printed planar phase correcting surface to improve directive radiation characteristics of electromagnetic band gap resonator antennas," *IEEE Trans. Antennas Propag.*, vol. 64, no. 1, pp. 276–280, Jan. 2016.
[48] M. A. Jamlos, W. A. Mustafa, W. Khairunizam, I. Zunaidi, Z. M. Razlan, and A. B. Shahriman, "Tumor detection via specific absorption rate technique using ultra-wideband antenna," *IOP Conf., Mater. Sci. Eng.*, vol. 557, no. 1, Jun. 2019, Art. no. 012024.

DEMYANA A. SALEEB received the B.Sc. degree (Hons.) in electronics and communication engineering from Modern Science and Arts (MSA) University, and the M.Sc. degree in electronics and communications engineering and the Ph.D. degree in applications of electromagnetic band gap (EBG) materials for the enhancement of antennas properties from the Faculty of Electronic Engineering, Menouf, Egypt. Her thesis was on "Transmission Line Modeling Method and Applications to Antennas." She is currently a Lecturer with the Department of Physics and Engineering Mathematics, Faculty of Engineering, Kafr Elshiekh University, Egypt. Her research interests include EBG materials, computational electromagnetics, and energy harvesting. She is a member of Engineering Syndicate, Egypt, and the Institution of Engineering and Technology (IET), U.K.

REHAB M. HELMY received the B.Sc. degree in electronics and communications from the Department of Electronics and Communications Engineering, Faculty of Engineering, Mansoura University, and the M.Sc. degree from Mansoura University, in 2015. She is currently pursuing the Ph.D. degree in communication engineering with the Faculty of Electronic Engineering, Menoufia University, Minuf, Egypt. Her thesis was on "Applications of Electromagnetic Bandgap Structures in Antenna." Her research interests include biomedical engineering and microwave applications.

NIHAL F. F. AREED received the B.Sc. degree (Hons.) in electronics and communications from the Department of Electronic and Communication, Faculty of Engineering, Mansoura University, in May 2000, and the M.Sc. and Ph.D. degrees in electrical communications from the Faculty of Engineering, Mansoura University, in 2003, and 2008, respectively. In January 2001, she was appointed as a Demonstrator with the Department of Electronics and Communications, Mansoura University. She was appointed as a Lecturer, in April 2008, an Associate Professor, in September 2013, and finally as a Professor, in September 2018. Her research interests include microwave and antenna, optical fibers, and plasmonic models. She is a member of IEEE Communication Society and OSA. She won the title of the Ideal Student of the Faculty of Engineering, in 1999. She was awarded the Scientific Excellence Award by the Egyptian Society of Engineers, in 2001. She won the State Incentive Award from the Academy of Scientific Research, in July 2018.

MOHAMED MAREY (Senior Member, IEEE) received the M.Sc. degree in electrical engineering from Menoufia University, Egypt, in 1999, and the Ph.D. degree in electrical engineering from Ghent University, Belgium, in 2008. From 2009 to 2014, he was a Research Associate and a Visiting Professor with the Faculty of Engineering and Applied Science, Memorial University, Canada. He is currently a Full Professor with the Faculty of Electronic Engineering, Menoufia University, Egypt. He is on a sabbatical leave in order to join Prince Sultan University, Saudi Arabia, as a Research Laboratory Leader of the Smart Systems Engineering Laboratory. He authored the book *Multi-Carrier Receivers in the Presence of Interference: Overlay Systems* (VDM Publishing House Ltd., 2009) and around 100 scientific papers published in international journals and conferences. His research interests include wireless communications and digital signal processing, with a particular focus on smart antennas, cooperative communications, signal classification for cognitive radio systems, synchronization and channel estimation, multiple-input multiple-output antenna systems, multicarrier systems, and error correcting codes. He was a recipient of the Young Scientist Award from the International Union of Radio Science, in 1999. He serves as an Editor for the IEEE Open Journal of the Communications Society.

KHALED MOHAMAD ALMUSTAFA received the B.E.Sc. degree in electrical engineering, and the M.E.Sc. and Ph.D. degrees in wireless communication from the University of Western Ontario, London, ON, Canada, in 2003, 2004, and 2007, respectively. He is currently working as a Professor with the Department of Information Systems (IS), College of Computer Science and Information Sciences (CCIS), Prince Sultan University (PSU), Riyadh, Saudi Arabia. He worked as a General Supervisor for the Information Technology and Computer Services Center (ITCS), PSU, the Chairperson of the Department of Communication and Networks Engineering (CME), the Vice Dean for the College of Engineering, PSU, the Director of the Research and Initiatives Center, PSU, and the CITO at PSU. His research interests include error performance evaluation of MIMO communication systems in partially known channels, adaptive modulation, and channel security, text recognition models, control systems with renewable energy applications, data prepossessing, and machine learning and computer vision.

AHMED S. ELKORANY received the B.Sc. degree (Hons.) in electronics and electrical communications and the M.Sc. and Ph.D. degrees in electrical communications (microwaves and antennas) from the Department of Electronics and Electrical Communications Engineering, Faculty of Electronic Engineering, Menoufia University, in 2003, 2007, and 2011, respectively. He was appointed as a Demonstrator, in December 2003. In December 2011, he was appointed as a Lecturer, and later as an Associate Professor with the Department of Electronics and Electrical Communications Engineering, Menoufia University, in August 2018. His research interests include numerical techniques, CAD tools, programming languages, UWB antennas and systems, EBG structures, wireless sensor networks and cognitive radio, metamaterials, the IoT, mobile antennas, and image processing.